

● *Original Contribution*

THEORETICAL AND EXPERIMENTAL CHARACTERISATION OF MAGNETIC MICROBUBBLES

HELEN MULVANA,* ROBERT J. ECKERSLEY,* MENG-XING TANG,[†] QUENTIN PANKHURST,[‡]
and ELEANOR STRIDE[§]

*Department of Imaging Sciences, Imperial College London, London, United Kingdom; [†]Department of Bioengineering, Imperial College London, London, United Kingdom; [‡]Davy-Faraday Research Laboratory, Royal Institution of Great Britain, London, United Kingdom; and [§]Department of Mechanical Engineering, University College London, London, United Kingdom

(Received 29 September 2011; revised 26 January 2012; in final form 27 January 2012)

Abstract—In addition to improving image contrast, microbubbles have shown great potential in molecular imaging and drug/gene delivery. Previous work by the authors showed that considerable improvements in gene transfection efficiency were obtained using microbubbles loaded with magnetic nanoparticles under simultaneous exposure to ultrasound and magnetic fields. The aim of this study was to characterise the effect of nanoparticles on the dynamic and acoustic response of the microbubbles. High-speed video microscopy indicated that the amplitude of oscillation was very similar for magnetic and nonmagnetic microbubbles of the same size for the same ultrasound exposure (0.5 MHz, 100 kPa, 12-cycle pulse) and that this was minimally affected by an imposed magnetic field. The linear scattering to attenuation ratio (STAR) was also similar for suspensions of both bubble types although the nonlinear STAR was ~50% lower for the magnetic microbubbles. Both the video and acoustic data were supported by the results from theoretical modelling. (E-mail: eleanor.stride@eng.ox.ac.uk) © 2012 World Federation for Ultrasound in Medicine & Biology.

Key Words: Magnetic microbubbles, Ultrasound, High speed camera, Magnetic nanoparticles, Ultrasound contrast agents, Gene therapy, Drug delivery.

INTRODUCTION

The use of ultrasound in combination with microbubble contrast agents has been widely demonstrated as a means of improving the delivery of drugs and genes *in vitro* and *in vivo* (Bekeredjian et al. 2005; Hernot et al. 2008). The technique offers considerable potential for the targeted treatment of a wide range of diseases including several types of cancer and both hereditary and acquired conditions. Progress from pre-clinical models to clinical application of the techniques has, however, been limited by the relatively low delivery efficiencies achieved. Several studies have sought to address this limitation through *in vitro* optimisation of the acoustic parameters (Karshafian et al. 2009; Rahim et al. 2006) and/or the type of microbubble employed (Li et al. 2003); but to

date the results have not translated into efficiency gains *in vivo* (Kinoshita et al. 2007; Li et al. 2009). Another approach has been to simply increase the dose of microbubbles delivered (Alter et al. 2009; Rahim et al. 2006). It is thought that this increases the probability of a sufficient number of microbubbles being sufficiently close to a given cell in the target region to generate a permeabilisation effect, thus, resulting in higher delivery efficiencies. This has been successfully demonstrated *in vivo*, but unfortunately, the extent to which the correlation between microbubble dose and delivery efficiency can be exploited clinically is limited by the associated risk of embolism with increasing microbubble dose (Alter et al. 2009). Attaching targeting species to the surface of microbubbles offers a means of manipulating microbubble concentration and proximity to target cells without increasing the overall dose administered. This has been investigated widely both for molecular imaging and therapeutic applications as detailed in the extensive review by Klibanov (Klibanov 2007). Despite a large number of studies being conducted in this area, however,

Address correspondence to: Eleanor Stride, Institute of Biomedical Engineering, Department of Engineering Science, University of Oxford, Old Road Campus Research Building, Oxford OX3 7DQ, UK. E-mail: eleanor.stride@eng.ox.ac.uk

the development of targeted microbubbles with sufficient specificity *in vivo* to ensure that a high proportion is not “wasted” on nontarget tissues is still proving challenging (Kooiman 2011).

An alternative and potentially complementary strategy, which has been demonstrated in previous work by the authors and another independent study, is to use microbubbles loaded with magnetic nanoparticles whose location can be manipulated using an externally applied magnetic field. Enhanced transfection has been demonstrated *in vitro* and *in vivo* (Stride *et al.* 2009; Mulvana *et al.* 2010b; Vlaskou *et al.* 2010). As above, it was hypothesised that the increased transfection rates were due to the increase in both concentration and proximity of the microbubbles to the target cells produced by the magnetic field. Further investigation to fully understand the mechanisms of enhancement and, hence, optimise the delivery protocols is, however, required. One question which was not addressed in the previous studies was whether or not the magnetic nanoparticles significantly affected the behaviour of the microbubbles. Similarly, the effect of placing the microbubbles in a magnetic field was also not examined explicitly. The aim of this study was to determine the influence of these factors on a range of microbubble characteristics, in particular their dynamic and acoustic response; and to relate these findings to a theoretical description of microbubble behaviour and the results of the previous *in vitro* and *in vivo* studies.

THEORETICAL DESCRIPTION

It is well known that upon exposure to ultrasound a microbubble will undergo volumetric oscillations due to the variations in pressure with time at a given location. These oscillations generate a secondary acoustic field and also motion of the liquid surrounding the microbubble. The former determines the signal or echo that may be detected by an ultrasound scanner; and there is evidence that the latter may be an important factor in mediating therapeutic effects, in particular the steady “microstreaming” produced in the immediate vicinity of an oscillating bubble (Marmottant *et al.* 2008). The exact mechanism(s) by which drug/gene delivery is enhanced and the corresponding features of bubble behaviour have still yet to be determined conclusively. In addition to microstreaming, microbubbles exhibit a number of other phenomena including nonspherical modes of oscillation, fragmentation and the emission of high speed liquid “microjets” (Vos *et al.* 2008, 2011; Chen *et al.* 2011; Postema *et al.* 2004). Accurate modelling of these phenomena in general requires the use of computationally intensive techniques such as boundary or finite element analysis, which are outside the scope of

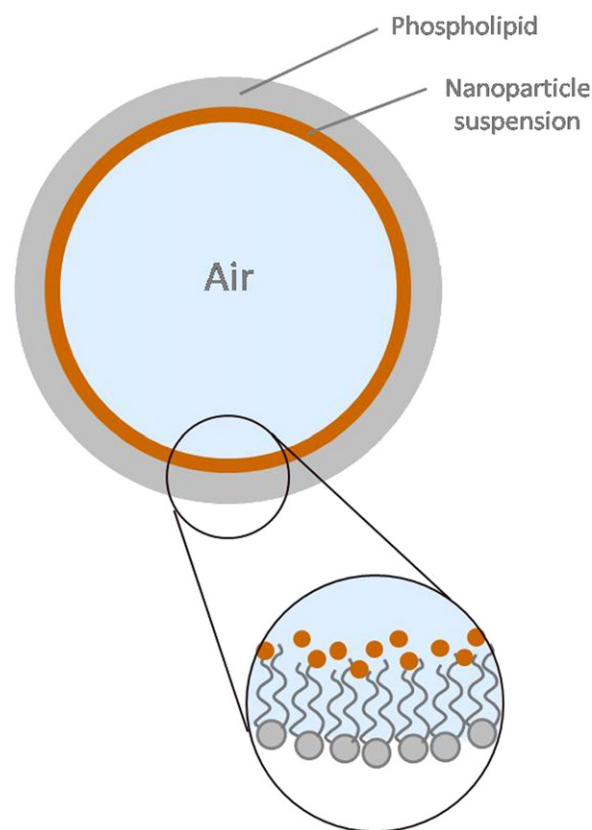


Fig. 1. Schematic of the structure of a magnetic microbubble.

this study (Qin *et al.* 2006; Martynov *et al.* 2009). It is relatively straightforward, however, to derive a model describing spherically symmetric bubble (volume) oscillations to examine the influence of an additional layer of magnetic nanoparticles; and importantly, this type of model can still provide useful insights since the amplitude of volumetric oscillations has been shown to be positively correlated with microstreaming intensity (Marmottant *et al.* 2008) and, at higher ultrasound pressures, the likelihood of *e.g.*, microjet formation.

To describe the volume oscillations of the magnetic microbubbles used in this and previous studies, a single bubble is modelled as a gas-filled sphere of radius R_1 , surrounded by a layer of viscous, hydrophobic liquid containing a fixed volume fraction, α , of solid spherical nanoparticles and onto which a surfactant (phospholipid) monolayer of negligible thickness is adsorbed (Fig. 1). Each bubble is considered to be suspended in isolation in an infinite volume of incompressible Newtonian viscous liquid having uniform constant density ρ_L and dynamic viscosity μ_L . Assuming mass is conserved and that there is continuity of stress at the internal and external bubble boundaries then following Church (1995) and integrating the equation for conservation of momentum in spherical polar coordinates gives:

$$\begin{aligned}
& \rho_s R_1 \ddot{R}_1 \left(1 + \frac{R_1}{R_2} \left(\frac{\rho_L - \rho_s}{\rho_s} \right) \right) \\
& + \rho_s \dot{R}_1^2 \left(\frac{3}{2} + \frac{R_1}{R_2} \left(\frac{\rho_L - \rho_s}{\rho_s} \right) \left(\frac{4R_2^3 - R_1^3}{2R_2^3} \right) \right) \quad (1) \\
& = p_A - p_0 + p_G - \frac{2\sigma_o}{R} - \frac{4\dot{R}_1 R_1^2}{R_2^3} \mu_L - \frac{4\dot{R}_1 \mu_s V_s}{R_2^3 R_1} - f(\Gamma)
\end{aligned}$$

where superscripted periods represent differentiation with respect to time, R_2 is the outer radius of the microbubble, $\rho_s = ((1-\alpha)\rho_o + \alpha\rho_{np})$, ρ_o is the density of the liquid in which the nanoparticles are suspended and ρ_{np} is the density of the magnetic nanoparticles themselves. μ_s is the viscosity of the nanoparticle suspension (the effects of nanoparticle interaction have been neglected in this model since the volume fractions considered are relatively low and distributed in a layer of finite thickness, thus, “jamming” of the particles is unlikely at moderate amplitudes of oscillation), $V_s = R_2^3 - R_1^3$, p_0 is the ambient pressure, $p_A(t)$ is an imposed pressure field (for which it is assumed the wavelength is large compared with the bubble radius), p_G is the pressure of the gas inside the bubble (assumed to behave polytropically *i.e.*,

$$p_G = p_0 \left(\frac{R_{01}}{R_1} \right)^{3\kappa}$$

κ is the polytropic constant and R_{01} is

the initial value of the gas core). For the sake of simplicity, the effects of static interfacial tension are neglected since these terms will be negligibly small. $f(\Gamma)$ represents the effect of the outer phospholipid coating upon the microbubble response, which is a function of the surface molecular concentration, Γ (Glazman 1983; Sarkar et al. 2005; Marmottant et al. 2005). $f(\Gamma)$ may take various forms and the detailed derivation for the equation of motion of a surfactant coated bubble with an internal liquid layer may be found in Stride (2008). For the purposes of this study, a simple linear form similar to that used by Sarkar et al. (2005) and Marmottant et al. (2005) was

$$\text{assumed, so that: } f(\Gamma) = \frac{4\eta_{s0}\dot{R}_2}{R_2^2} + \frac{2K}{R_2} \left(1 - \left(\frac{R_{02}}{R_2} \right)^2 \right)$$

where R_{02} is the initial outer radius of the bubble and η_{s0} and K are constants for a given surfactant. The first term characterises the surface viscosity imparted by the surfactant coating. The second term relates to the variation in surface tension with molecular concentration as the bubble oscillates. The pressure radiated by the bubble can then be found as (Leighton 1994):

$$p_{rad}(r, t) = \rho_L \left(\frac{1}{r} \left(R_2^2 \ddot{R}_2 + 2R_2 \dot{R}_2^2 \right) - \frac{R_2^4 \dot{R}_2^2}{2r^4} \right) \quad (2)$$

To fully capture the nonlinear behaviour of the bubbles, eqns (1) and (2) were solved numerically using a fourth order Runge-Kutta solver (function ode45) in

Matlab (version 7, release 14; The Mathworks, Natick, MA, USA) for the range of bubble sizes and exposure conditions relevant to the experiments described in the next section.

This study is concerned primarily with the dynamic and acoustic response of individual microbubbles on the timescale of an ultrasound pulse ($\sim 1-10 \mu\text{s}$). The theoretical treatment, therefore, neglects the effects of bubble translation under flow, acoustic radiation force or due to a magnetic field since these will occur on a relatively long timescale. These effects, together with multiple bubble interactions, are, however, of great significance in the development of treatment protocols using magnetic microbubbles and will be discussed later.

EXPERIMENTAL CHARACTERISATION

Microbubble fabrication

The method used for preparing magnetic microbubbles is described in detail in Stride et al. 2009. Briefly, 15 mg of a phospholipid (hydrogenated L- α -phosphatidylcholine purchased from Sigma-Aldrich, Poole, Dorset, UK) were added to 15 mL of filtered deionised water at room temperature through which perfluoropropane (C_3F_8) gas had been bubbled. The lipid was dispersed by sonication for 30 s using an ultrasonic cell disruptor (XL2000, probe diameter 3 mm; Misonix Inc., Farmingdale, NY, USA) operating at 22.5 kHz and level 4 corresponding to 8 W output power. A quantity of 15 μL of a suspension of 10 nm diameter superparamagnetic nanoparticles in a hydrocarbon carrier liquid (Liquids Research, Bangor, UK) was then added and the mixture sonicated again under the same conditions but during the second sonication the probe was raised and lowered to and from the liquid surface to entrain gas. Following sonication, the mixture was immediately manually shaken vigorously for 30 s. For comparison, suspensions of nonmagnetic microbubbles were also prepared. The same technique was used but without the addition of the magnetic nanoparticle suspension and only a single sonication step. This method was selected because it produces a high yield of microbubbles with a size distribution comparable to that found in commercial contrast agents. As will be discussed later, however, there are disadvantages that may be overcome by the use of alternative fabrication techniques.

Optical characterisation

Directly after fabrication, the microbubble suspensions were examined in a haemocytometer under an optical microscope (Nikon Eclipse 50i; Nikon Instruments Europe B.V., Surrey, UK) to establish their size distribution and concentration. The suspensions were gently agitated to ensure their homogeneity before

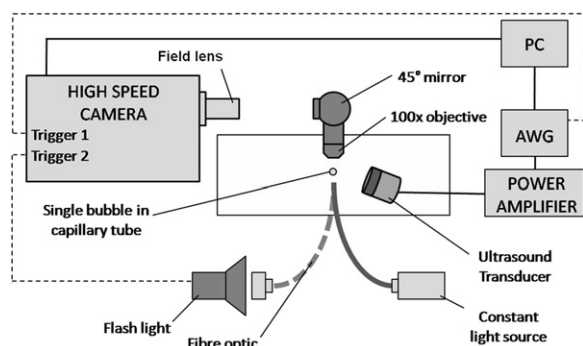


Fig. 2. Experimental apparatus used for high speed video microscopy.

10 μL of the suspension was extracted using a micropipette and injected into the haemocytometer chamber. Twenty images were captured from three samples for each suspension and analysed using a program developed in Matlab (The Mathworks Inc.) specifically for this purpose and described in Sennoga *et al.* (2010). It was also verified during the microscopic examination that a sufficient quantity of magnetic material had been incorporated into the bubbles to allow them to be manipulated by application of a permanent magnet to the side of the microscope stage.

Acoustic response

High speed video microscopy. To study the oscillatory behaviour of different types of bubble (*i.e.*, magnetic and nonmagnetic), high speed video microscopy was used to record the change in radius of a single bubble in response to ultrasound excitation. These experiments provide data that can be compared with the results from the theoretical modelling [eqn (1)].

A diagrammatic representation of the apparatus used is shown in Figure 2. A dilute suspension of microbubbles was injected into a 200 μm diameter cellulose capillary (Membrana GmbH, Hamburg, Germany) immersed in a water bath held at 37°C and illuminated from below using a fibre-optic light source. The capillary tube was visualized using a 100x submersible microscope objective (LUMPlan FL \times 100; Olympus UK Ltd, Essex, UK) projected onto a viewing plate and a micrometre precision translation stage (562 Series ULTRAlign; Newport, Didcot, UK) was used to focus the image and scan along the length of the tube to locate single, isolated bubbles. The bubble image was optically coupled *via* a plano-convex ($f = 50$ mm) lens (Thorlabs Ltd., Cambridgeshire, UK) and field lenses (Nikon ED AF Nikkor 70–300 mm; Nikon, Tokyo, Japan and 70-300 field lens, respectively) to the Cordin 550 fast-framing camera (Cordin, Salt Lake City, USA).

Single bubbles were excited with a 0.5 MHz single element focused transducer ($f = 40$ mm) (Videoscan V301; Panametrics, Olympus-NDT, Waltham, MA, USA), positioned so that the acoustic focus was coincident with the optical focus of the microscope objective within the capillary tube. The transducer was driven with a 12-cycle, 0.5 MHz, Gaussian windowed pulse to develop a moderate (c.100 kPa, MI 0.14) peak negative pressure at the focus. Signals were defined in Matlab and uploaded to an arbitrary signal generator (AWG2021; Tektronix, Bracknell, UK) before power amplification (2100L power amplifier; E & I Ltd, Rochester, NY, USA). It should be noted that it was necessary to use a relatively low ultrasound frequency due to the maximum camera frame rate available (~ 2.5 Mfps). Consequently the larger microbubbles in the population, which would be resonant at approximately this frequency, were selected for these experiments.

Data were acquired for the following: magnetic bubbles, nonmagnetic bubbles and also a commercial contrast agent, SonoVue® (Bracco Suisse S.A., Geneva, Switzerland). In addition, the response of the magnetic bubbles was recorded in the presence of a permanent magnet (rectangular block 10 mm \times 310 mm \times 325 mm N52 grade NdFeB, transversal magnetisation 1.5 T; NeoTexx, Berlin, Germany) mounted on a rotating arm, which allowed it to be translated towards and away from the capillary fibre. For each microbubble studied, a series of 58 images were recorded at 2.5 million frames per second (Mfps) with a final image resolution of 20 pixels per micrometre. Images were downloaded to a PC for postprocessing in Matlab and analyzed using custom segmentation software developed specifically for this purpose to record the bubble diameter as a function of time. The images were also used to generate a video file to allow other features of the microbubble oscillation to be examined.

Scattering to attenuation ratio (STAR). To quantify the acoustic response of the different microbubble populations, acoustic scattering and attenuation measurements were performed using the apparatus and procedure previously described in Mulvana *et al.* (2010a). A sufficient volume of microbubbles to generate approximately 50% attenuation of the total transmitted signal was suspended in 300 mL filtered, gas-saturated, deionised water held at 37°C to approximate *in vivo* conditions in a chamber with parallel acoustically transparent windows consisting of 6 μm thick polyester film (Goodfellow Cambridge Ltd., Cambridge, UK). The chamber was immersed in a water bath also at 37°C, at the mutual focus of a pair of single element 3.5 MHz transducers aligned with their axes perpendicular and having a focal length of 75 mm and full-width-half-maximum bandwidth 2.08–5.72 MHz (Videoscan V380; Panametrics, Olympus-NDT).

Table 1. Microbubble suspension characteristics

| | Mean diameter (μm) | Bubble concentration (bubbles/mL) | Gas concentration ($\mu\text{L/mL}$) |
|--------------------------|---------------------------------|----------------------------------------|----------------------------------------|
| Magnetic microbubbles | 1.2 ± 0.03 | $3.7 \times 10^8 \pm 0.9 \times 10^8$ | 0.65 ± 0.18 |
| Nonmagnetic microbubbles | 1.9 ± 0.12 | $0.5 \times 10^8 \pm 0.06 \times 10^8$ | 0.54 ± 0.26 |
| SonoVue® | 2.5 | $2 - 5 \times 10^8$ | 8 |

It should be noted that the data for SonoVue® are taken from Gorce et al. (2000) and correspond to the suspension as prepared according to the manufacturer's instructions.

One transducer was driven with a mirrored stepped pressure ramp made up of a series of pulse-inversion (PI) pairs with the pulse in each case consisting of a two-cycle Gaussian windowed sinusoid with centre frequency 3.5 MHz over a pressure range from 22–217 kPa in 30 kPa increments. As for the single bubble measurements, the signals were generated in Matlab and uploaded to an arbitrary signal generator (AWG2021, Tektronix) before power amplification (2100L; E & I Ltd.). The scattered signals were received using the second, matched transducer positioned so that its focus was coincident with the transmit device, whilst the attenuated signals were acquired in the far field using a 1 mm diameter needle hydrophone (Precision Acoustics Ltd., Dorset, UK) aligned coaxially with the first transducer. A pulse repetition frequency (PRF) of 2 Hz was used for a total of 50 bursts, while the PRF between the incremented pressure ramp pulses was 5 kHz. The microbubble suspension was briefly stirred manually after the microbubbles were added and following each data acquisition. Following each set of measurements, the chamber was flushed and refilled with a fresh bubble suspension. Measurements were repeated three times to obtain an average value in each case.

All received signals were amplified using a pulser-receiver (5800; Panametrics, Olympus-NDT), operating in receive mode before acquisition *via* a digitizer to a PC for post-processing in Matlab to recover the attenuation, total scattered and nonlinear scattered component in each case. The nonlinear content of the scattered signal was obtained through pulse inversion. Corresponding positive and negative pulse inversion pairs were summed at each pressure to cancel the linear component of the pulse, leaving a mirrored pressure ramp of residual pulses for further processing. The mean pulse-inverted residual signal was calculated over 50 repeats at each pressure using a fast Fourier transform of the windowed (Hamming) signals. In each case, the amplitude spectra were calculated with reference to the background noise, so that measurements were in decibels greater than the background signal for a given acoustic excitation pressure and then used to calculate the scattering to attenuation (STAR) and nonlinear STAR (nSTAR) ratios. These ratios provide a means of assessing the efficiency of contrast agents (Bouakaz et al. 1998).

RESULTS

Optical characterisation

The measured size distributions and concentrations of the magnetic and nonmagnetic microbubbles are shown in Table 1 and Figure 3. For comparison, information for the commercial ultrasound contrast agent, SonoVue® is also shown (Gorce et al. 2000). As may be seen, the concentration of microbubbles was considerably higher for the magnetic than for the nonmagnetic microbubbles. It is possible that this was due to the

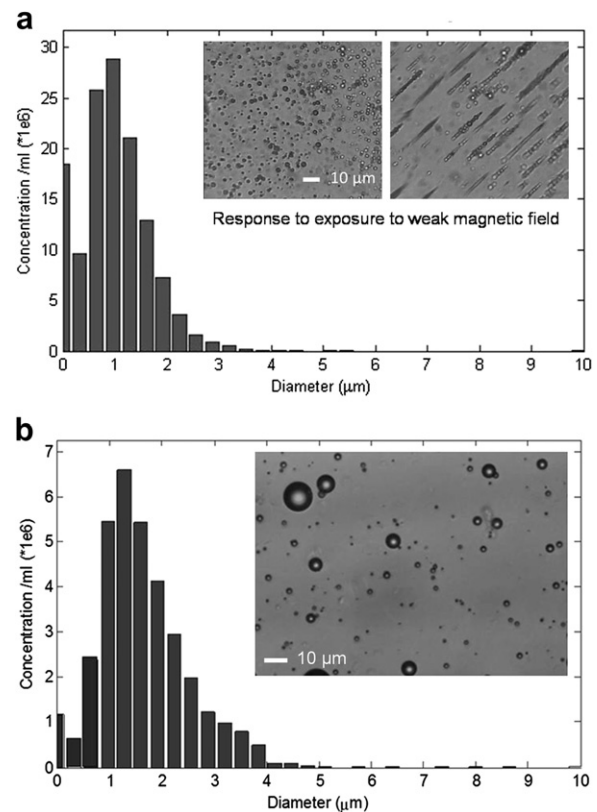


Fig. 3. Size distributions for (a) magnetic and (b) nonmagnetic microbubbles determined *via* optical microscopy for three sets of 20 micrographs. Inserts show optical micrographs of the corresponding microbubble suspensions. The right hand image of the magnetic bubbles was obtained after holding a 1.5 T permanent magnet at the edge of the haemocytometer for approximately 10 s.

nanoparticles or droplets of the nanoparticle suspension acting as nucleation sites within the liquid, since it is well known that hydrophobic particles will encourage the formation of bubbles during exposure to ultrasound (Apfel 1984). The difference in concentration was not due to the fact that the nonmagnetic microbubbles were prepared with only a single sonication step. Repeating the sonication was actually found to reduce the concentration further. The mean size of the magnetic microbubbles was also different, being slightly smaller than for the nonmagnetic bubbles (which were themselves similar in size to SonoVue® microbubbles). Both this and the fact that the polydispersity index (standard deviation: mean diameter) was lower for the magnetic microbubbles (0.025 opposed to 0.06) could also be explained in terms of the nanoparticles suspension promoting bubble formation. Nevertheless, although similar results were obtained for each batch of microbubbles in this study, the relatively high degree of variability inherent in bulk agitation methods for microbubble preparation should also be borne in mind.

The visual appearance of the microbubbles was also different, with the magnetic microbubbles having a different colouring (brownish tint) from the nonmagnetic microbubbles. The latter were, however, indistinguishable visually from SonoVue®. It was also clear from visual inspection that the magnetic microbubble suspension, as made, contained more than one type of particle. The “true” magnetic microbubbles for which the data are shown in Table 1, Figure 3 and subsequent figures were identified by the fact that they were both buoyant and responsive to a magnetic field. These characteristics provided a means of separating them from the remainder of the suspension. Also present, however, were buoyant bubbles, which were not magnetically responsive and nonbuoyant particles which were. It was assumed that these corresponded respectively to microbubbles containing little or no magnetic material and lipid stabilised droplets of the magnetic nanoparticle suspension containing little or no gas. This was confirmed by their acoustic response as described below.

Differences in the response to an imposed magnetic field also indicated that within the magnetic microbubble population there was some variation in the quantity of magnetic material encapsulated in each microbubble. As, will be discussed later, this was reflective of the bulk nature of the fabrication method used that provided no direct control over individual microbubble composition. Similar to other types of magnetic particle the microbubbles were observed to form chains in the presence of a magnetic field that then behaved as single entities *e.g.*, translating and/or rotating in response to changes in the field (Fig. 3a). Neither the nonmagnetic nor

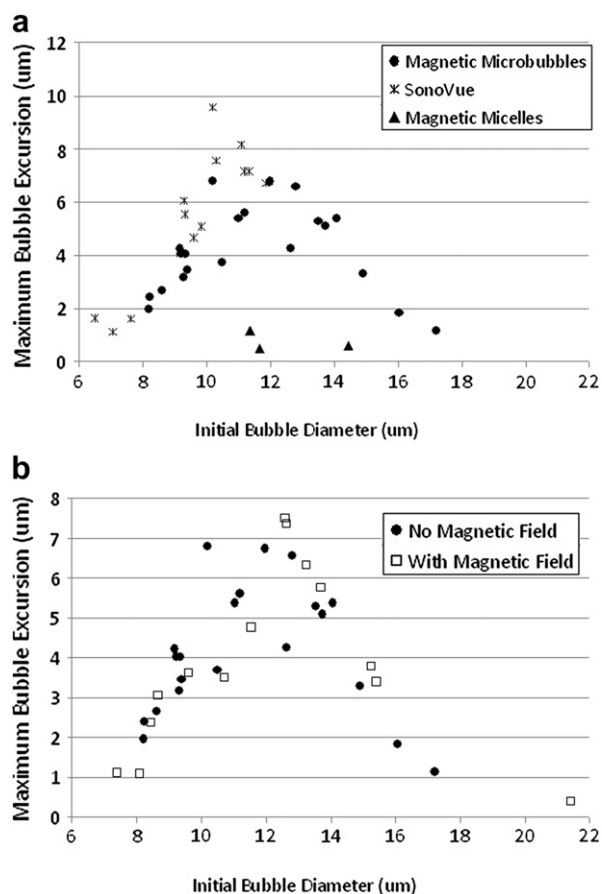


Fig. 4. Microbubble response to ultrasound excitation (12-cycle, 0.5 MHz, Gaussian windowed pulse ~ 100 kPa focal peak negative pressure). Variation in the amplitude of radial expansion with initial bubble diameter as measured from the high speed camera footage for (a) different types of microbubbles (b) with and without an imposed magnetic field.

SonoVue® microbubbles showed any response to the magnetic field as would be expected.

Single bubble response

Figures 4a and b show respectively how the maximum amplitude of radial oscillation varied with initial size for the different types of microbubble studied and with and without the presence of a magnetic field.

Effect of magnetic nanoparticle loading. As may be seen, the response of the magnetic microbubbles was found to be similar to that of the nonmagnetic bubbles, which was indistinguishable from that observed for SonoVue® microbubbles. For the sake of clarity, therefore, only the results for the magnetic microbubbles and SonoVue were plotted. The resonant size was slightly larger for the magnetic microbubbles and it was hypothesised that this was due to the fact that the resonant size is largely governed by the radius of the air core, which will

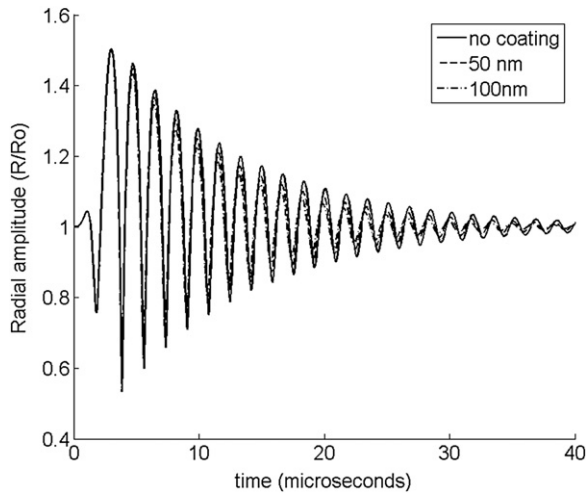


Fig. 5. Variation of microbubble radius with time in response to an ultrasound pulse for magnetic coating layers of different thicknesses as predicted by eqn (1). The following values were used in the calculations, which were performed in Matlab (v.7.0 The Mathworks): $R_{02} = 6.0 \times 10^{-6}$ m, $\rho_L = 1000$ kg m $^{-3}$, $\rho_o = 700$ kg m $^{-3}$, $\rho_{np} = 5100$ kg m $^{-3}$, $\alpha = 0.1$, $p_0 = 10^5$ Pa, $p_A = |p_A| \sin(2\pi ft) e^{-\frac{4(\nu-\tau)}{r}}$, $f = 0.5$ MHz, $|p_A| = 100$ kPa, $p_G = \left(p_0 + \frac{2\sigma_0}{R_{01}}\right) \left(\frac{R_{01}}{R_1}\right)^{3\kappa}$, $\sigma_0 = 0.05$ Nm $^{-1}$ $\kappa = 1$, $\mu_L = 10^{-3}$ Pas, $\mu_S = 10^{-2}$ Pas, $\eta_{s0} = 4.5 \times 10^{-9}$ kg s $^{-1}$, $K = 0.3$ N m $^{-1}$. The parameters relating to the magnetic liquid were based on its bulk properties as supplied by the manufacturer. Those relating to the lipid coating were based previous experiments performed by Chetty et al. (2008) with the same apparatus. The gas was assumed to be air and the surrounding liquid water. The coating parameter values were obtained by comparing equivalent terms in the linearised form of eqn (1) with those in eqns (1)–(3) in Chetty et al.

be different for magnetic and nonmagnetic bubbles due to the layer of magnetic material in the former.

The effect of the magnetic layer was investigated further through theoretical simulation. Figure 5 shows the effect of varying layer thickness on the amplitude of microbubble oscillations as predicted by eqn (1). As may be seen, the amplitude of oscillation was only slightly reduced by the presence of a layer of a few 10 s of nm in accordance with the experimental observations. The approximate thickness was based on results from electron microscopy (unpublished) and also the velocity at which microbubbles were seen to translate in response to a known magnetic force. (These results are not reported explicitly here as the full study is still in progress and only approximate estimates are currently available. It is for this reason that a range of shell thicknesses were modelled.) No attempt was made to fit the experimental data to the theoretical results to estimate the shell thickness, however. This was firstly on account of the uncertainty in the other parameters, which were based on results for other phospholipid coated bubbles (Chetty

et al. 2008) and, hence, the potential nonuniqueness of the fitting problem. Secondly, the fact that the microbubbles were confined in a capillary and adjacent to its inner surface meant that the assumption of an infinite liquid was invalidated and quantitatively accurate results could not, therefore, be obtained. In fact, the resonant diameter in Figure 4 (~ 11 μ m) corresponded very closely to that which would be predicted by the Minnaert equation [*i.e.*, the linear analytical solution to eqn (1) for an uncoated bubble] but it would be incorrect to make a direct comparison for the same reasons.

Effect of magnetic field. Figure 6 shows two sets of images from the high speed camera footage of a magnetic microbubble undergoing volumetric oscillations in response to ultrasound exposure with (a) and without (b) a permanent magnet held nearby. Within the bounds of uncertainty for the experiment (*i.e.*, image resolution and sensitivity of the edge detection algorithm) there was no appreciable difference between the behaviour of “free” microbubbles and those restrained using a magnetic field in terms of resonant diameter and amplitude of oscillation (Fig. 4b), or qualitative features of the oscillations such as nonsphericity, surface indentation as a precursor to jet formation etc. This was perhaps somewhat surprising but it should be considered that in both cases the microbubble was positioned in close proximity to the tube wall, either against the top surface due to buoyancy or the side due to the magnetic force; and for the magnet used, both forces would have been on the order of piconewtons (Stride et al. 2009 Appendix). Thus, the bubble environment was similar in both cases. A detailed analysis of the direction in which, *e.g.*, surface indentation occurred was not made since this would be difficult to perform with accuracy but a qualitative difference was seen corresponding to the different positions of the bubble. Ideally, images of the bubble oscillating in perpendicular image planes would be obtained (Vos et al. 2008, 2011).

Magnetic droplets. Also shown in Figure 4a are results for nonbuoyant particles extracted from the original magnetic microbubble suspension. As anticipated, they did not exhibit any observable response to ultrasound excitation regardless of their initial diameter supporting the conclusion that they were liquid droplets of the same magnetic nanoparticle suspension coated with phospholipid but containing negligible quantities of air. They would, thus, be unresponsive to ultrasound excitation.

Scattering and attenuation measurements

The results from the acoustic scattering and attenuation measurements from the microbubble suspensions (Table 2) were in agreement with the single bubble results in the sense that the linear STAR values obtained were

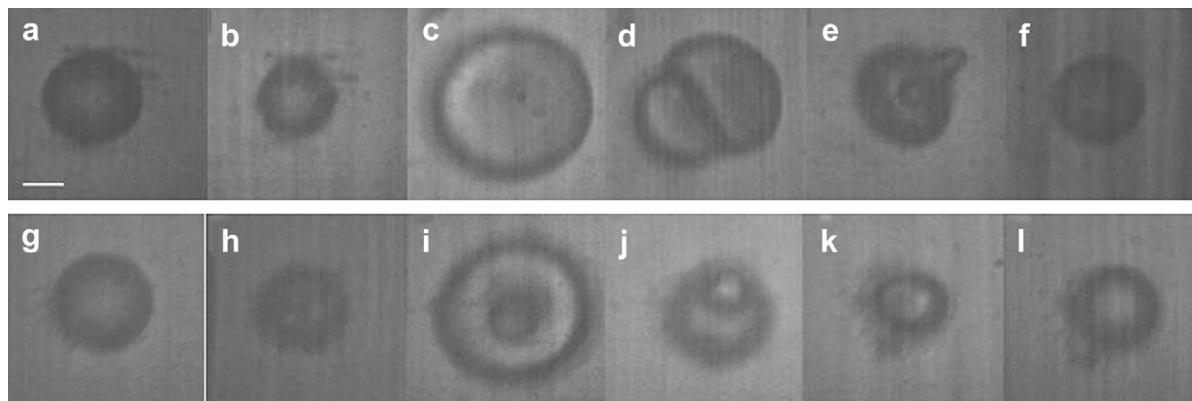


Fig. 6. Single frames from high speed camera video microscopy of a magnetic microbubble confined in a cellulose tube ($200\ \mu\text{m}$ inner diameter) under ultrasound excitation (c.f. Fig. 4). (a–f) Microbubble oscillations in the absence of a magnetic field. (g–l) Microbubble oscillations in the presence of a magnetic field. In each case the microbubbles had an initial diameter of $\sim 12.7\ \mu\text{m}$ (scale bar is $5\ \mu\text{m}$).

similar for both the magnetic and nonmagnetic bubbles, taking into account the large experimental uncertainty in the linear scattering measurements. An important point to note, however, is that the total volume of magnetic microbubbles ($390\ \mu\text{L}$) added to the measurement chamber was more than double that of the nonmagnetic microbubbles ($162\ \mu\text{L}$). This will be discussed in the next section.

In comparing the different sets of results it must be mentioned again that the frequencies for the single bubble and STAR measurements and the corresponding range of bubble sizes were different. As shown in Figure 7a, however, the theoretical simulations produced qualitatively similar results for smaller bubbles at higher frequencies. Figure 7b shows the corresponding frequency spectra for the radiated pressure for both bubble sizes and driving frequencies. As can be seen, whilst the change in radial amplitude is relatively small, the harmonic content of the radiated pressure becomes significantly reduced with increasing oil layer thickness again in accordance with the experimental results. (It should be noted that the bubble resonance frequency changes as the oil layer thickness changes and this accounts for the relative amplitudes of the radial oscillations in Fig. 5 and 7a.) This is in agreement with the fact that the

nonlinear scattering to attenuation ratio (nSTAR) measured was slightly lower for the magnetic microbubbles.

DISCUSSION

Previous studies (Stride *et al.* 2009; Mulvana *et al.* 2010b; Vlaskou *et al.* 2010) have demonstrated the potential use of magnetic microbubbles for therapeutic applications, both *in vitro* and *in vivo* and the aim of this study has been to address some of the questions raised by their findings. In this section, consideration is made of the implications of the results presented in the previous section in the context of the existing *in vitro/in vivo* results, further questions arising from the research and practical considerations for the development of a magnetic microbubble agent.

Nonlinear character

The fact that the amplitude of oscillation for the magnetic microbubbles was found to be similar to that for the nonmagnetic microbubbles for the same excitation conditions means that they will be detectable under conventional ultrasound imaging (and indeed this was confirmed as above). That the nonlinear character of the magnetic microbubble oscillations was less pronounced,

Table 2. Attenuation, linear and nonlinear scattering for magnetic and nonmagnetic microbubble suspensions exposed to two-cycle Gaussian windowed sinusoidal pulse inversion pairs with centre frequency 3.5 MHz over a pressure range from 22–217 kPa in 30 kPa increments

| | Mean attenuation | Mean linear scattering | Mean nonlinear scattering | STAR | nSTAR |
|----------------------------------------------------------|------------------|------------------------|---------------------------|------|-------|
| | dB | dB | dB | % | % |
| Magnetic microbubbles ($390\ \mu\text{L}$ in 300 mL) | 39.7 ± 8.4 | 0.87 ± 0.67 | 0.09 ± 0.01 | 2.18 | 0.22 |
| Nonmagnetic microbubbles ($162\ \mu\text{L}$ in 300 mL) | 47.3 ± 9 | 0.73 ± 0.64 | 0.24 ± 0.05 | 1.54 | 0.50 |

STAR = scattering to attenuation ratio; nSTAR = nonlinear scattering to attenuation ratio. Measurements are expressed in decibels relative to the background noise level.

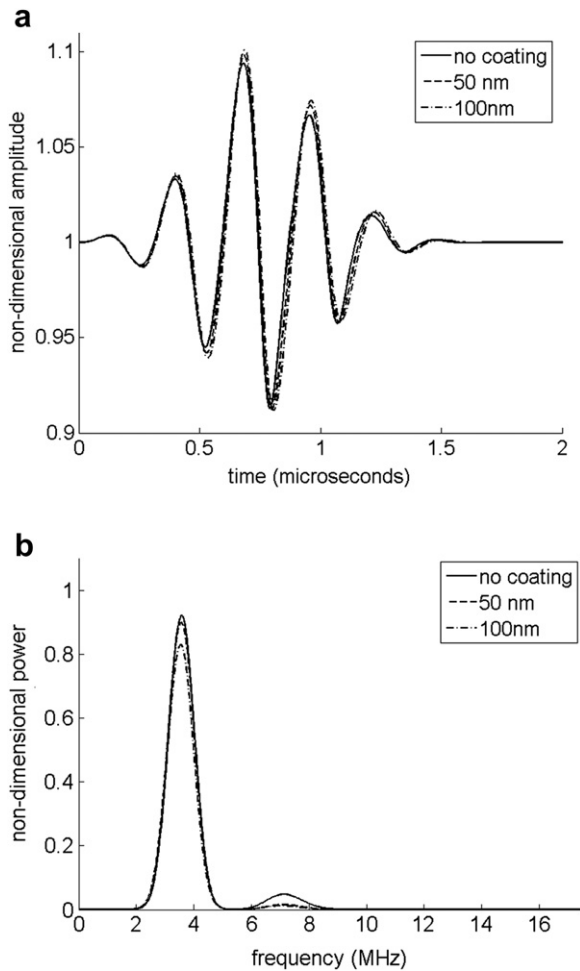


Fig. 7. Response of a magnetic microbubble to ultrasound excitation as predicted by eqn (1): (a) variation of microbubble radius with time in response to an ultrasound pulse for magnetic coating layers of different thicknesses (b) the corresponding frequency spectra for the radiated pressure from the microbubble showing the reduction in nonlinear content with increasing layer thickness. Calculation parameters as for Figure 5 except $R_{02} = 1.0 \times 10^{-6}$ m and $f = 3.5$ MHz.

however, is undesirable, since the contrast to tissue available with contrast specific imaging techniques will be lower. Other work on coated microbubbles has demonstrated that the nonlinear character can actually be enhanced by the presence of solid nanoparticles, provided they are confined to a thin layer at the bubble surface (Stride et al. 2008) and these findings should perhaps be taken into future development of magnetic microbubbles.

In the absence of clear evidence as to which phenomena are most important for promoting cell uptake and other bio-effects, it is not possible to determine whether the difference in nonlinear character has any implications for therapeutic applications. As above, there was no discernible difference in the tendency of the different bubble types to undergo nonspherical deformations at

the relatively moderate pressures used, although this may have been due to the limitations of the imaging system in terms of spatial resolution and the fact that images were only obtained in one plane as above. Considerably higher transfection efficiencies were observed in the previous *in vitro* studies with magnetic microbubbles but this may be attributed to the fact that the magnetic field produced higher local bubble concentrations, higher bubble/cell proximity and/or the contribution of magnetofection.

Microbubble preparation

Uniformity. Since the sonication preparation technique was found to produce a mixture of both magnetic and nonmagnetic microbubbles and magnetic droplets, additional processing steps were required to extract the magnetic microbubbles. This is clearly undesirable from a practical point of view and introduces uncertainty into the assessment of the microbubble size distribution and concentration. Differences in the response of individual microbubbles to the presence of a magnetic field and, to a lesser extent in their acoustic response, also indicated a lack of uniformity within the magnetic microbubble population. It is thought that this is the most likely explanation of the difference in the volume of microbubbles required to produce similar levels of attenuation and scattering (Table 2) *i.e.*, that despite the additional processing, only a proportion of the microbubbles added were sufficiently acoustically active.

For therapeutic applications in particular it is desirable to be able to maximise the number of bubbles present at a target location and to be able to predict *e.g.*, the amplitude of oscillation required to promote a given therapeutic effect. This requires microbubbles that are uniform both in terms of size and magnetic content. A number of recent studies have demonstrated the potential of alternative preparation techniques such as microfluidic processing to control microbubble size (*e.g.*, Talu et al. 2006). It has also been shown that the thickness of the microbubble coating can be varied systematically although so far this has only been demonstrated with polymer coated microbubbles and/or liquid droplets (Bohmer et al. 2006; Chang et al. 2010). Future work will, therefore, include investigating the use of different methods to prepare more uniform microbubble suspensions.

Size. A further advantage of using *e.g.*, a microfluidic processing technique is the ability to predetermine the size of the microbubbles. For vascular applications, the main restriction is that the outer diameter does not exceed $\sim 6 \mu\text{m}$ to ensure the microbubbles can pass through the capillary bed. In addition, it must be possible to incorporate sufficient material (therapeutic agent, magnetic nanoparticles etc.) to make the microbubbles functionally effective. Thirdly, the quantity of gas must be such that an

adequate acoustic/dynamic response can be obtained at ultrasound frequencies and pressures within the range that can be safely used clinically. It is known from previous studies that therapeutic efficacy is strongly influenced by the matching of ultrasound exposure conditions to the bubble acoustic response (Rahim *et al.* 2006). For nonvascular applications, it may be desirable to prepare smaller microbubble precursors containing a volatile liquid (variously referred to in the literature as phase-shift emulsions and acoustic droplet vaporization (ADV) (Zhang *et al.* 2011) that are able to undergo extravasation.

Composition. In the authors' original study of magnetic microbubbles (Stride *et al.* 2009), the components were deliberately selected to provide as simple a bubble composition as possible to minimise the sources of variability in the subsequent experiments. There have been numerous studies, however, on the composition of nonmagnetic microbubbles demonstrating the effect of different phospholipids upon microbubble stability, acoustic response, conjugation with therapeutic components and the addition of components such as polyethyleneglycol for improving biocompatibility (Borden *et al.* 2004). The results of these studies may be readily utilised in developing improved formulations. Microbubble stability was not studied explicitly in this work but is clearly a very important factor both for storage of the microbubbles and their transport *in vivo* and will be the subject of a separate investigation. There were negligible changes in the bubble size distributions obtained *via* optical microscopy over the time periods corresponding to the experiments in this study. Similarly, there was no incidence of bubble destruction in the high speed camera recordings.

Magnetic field

As discussed above, the response of individual microbubbles was not significantly affected by the presence of the magnetic field but it was observed that chain-like structures formed in microbubble populations. The effect of this upon the dynamic/acoustic response was not directly studied here but it is well known that bubbles behave differently in populations (Commander and Prosperetti 1989) and that microbubble concentration is strongly correlated to therapeutic efficacy and this does, therefore, require future investigation.

The strength and gradient of the magnetic field is also essential to successful localisation of microbubbles at a target site and determining the contribution of other effects such as magnetofection. The potential for magnetic localisation (of solid/liquid particles) has been demonstrated in various studies over the past few decades including at tissue depths relevant to human subjects (Widder *et al.* 1979). Localisation of magnetic microbub-

bles has so far been demonstrated only in a mouse model and careful consideration of the magnetic field strengths and gradients required at larger tissues depths is, therefore, required, taking into account the additional forces imposed due to blood flow and acoustic radiation force.

Safety

No adverse effects were reported in any of the previous studies on magnetic microbubbles *in vitro* or *in vivo* but much more extensive testing is clearly required. The mean size of the microbubbles prepared in this study is comparable with that of commercial contrast agents and no agglomeration has been observed in the absence of a magnetic field. The purpose in applying a magnetic field, however, is to increase the local concentration of microbubbles in a given region and this clearly increases the risk of embolism if the target region is not clearly defined. Iron oxide nanoparticles have already been approved for clinical use in humans as contrast agents for magnetic resonance imaging (MRI) but elimination and toxicity studies will still be required, especially if the concentrations used in magnetic microbubbles are higher.

SUMMARY AND CONCLUSIONS

Previous work has demonstrated that incorporating magnetic nanoparticles into phospholipid coated microbubbles provides a means of controlling microbubble location and concentration through the application of an external magnetic field. Increased efficiency has been demonstrated for gene delivery both *in vitro* and *in vivo* compared with that achieved using nonmagnetic microbubbles. The aim of this investigation was to study the physical characteristics and behaviour of magnetic and nonmagnetic microbubbles to better understand the mechanism(s) underlying this enhancement. The results indicate that both the physical properties of the microbubble suspension (size, size distribution and concentration) and their response to acoustic excitation are only affected to a small degree by the presence of the magnetic nanoparticles. Examination of microbubble suspensions under optical microscopy indicated that the mean size was slightly smaller (1.2 μm vs. 1.9 μm), the size distribution narrower (0.03 μm vs. 0.12 μm standard deviation) and the concentration higher for magnetic microbubbles (0.65 vs. 0.54 $\mu\text{L/mL}$). This was attributed to the hydrophobic nature of the magnetic nanoparticles suspension promoting bubble formation during fabrication by sonication. High speed video microscopy indicated that the amplitude of oscillation was very similar for magnetic and nonmagnetic microbubbles of the same size under the same ultrasound exposure conditions, with the resonant diameter being slightly larger for the former

($\sim 12 \mu\text{m}$ compared with $\sim 11 \mu\text{m}$ at 0.5 MHz). This would be expected since, for a fixed outer diameter, the inner gas core would be slightly smaller due to the presence of the layer of magnetic material. The acoustic scattering and attenuation measurements also indicated that both types of microbubble exhibited a similar response, with that of the magnetic microbubbles being somewhat more linear (STAR ratio for harmonic signal content was approximately 50% smaller). Both the high speed video and acoustic data were supported by the results from theoretical modelling of a spherical phospholipid coated microbubble with and without a viscous liquid layer. Future work will focus on the refinement of the fabrication methodology for the purposes of increasing microbubble concentration and uniformity, improving the nonlinear character of the microbubble response and further assessment for ongoing *in vivo* testing.

Acknowledgments—The authors would like to thank the Engineering and Physical Sciences Research Council (EPSRC) Loan Pool for provision of the high speed camera and in particular Adrian Walker for his assistance; The EPSRC and The Leverhulme Trust for their support respectively through grant EP/F066740/1 and the Philip Leverhulme prize awarded to Dr. Stride.

REFERENCES

- Alter J, Sennoga CA, Lopes DM, Eckersley RJ, Wells DJ. Microbubble stability is a major determinant of the efficiency of ultrasound and microbubble mediated *in vivo* gene transfer. *Ultrasound Med Biol* 2009;35:976–984.
- Apfel RE. Acoustic cavitation inception (Acoustic cavitation series: Part four). *Ultrasonics* 1984;22:167–173.
- Bekeredjian R, Grayburn PA, Shohet RV. Use of ultrasound contrast agents for gene or drug delivery in cardiovascular medicine. *J Am Coll Cardiol* 2005;45:329–335.
- Bohmer MR, Schroeders R, Steenbakkers JAM, de Winter SHPM, Duineveld PA, Lub J, Nijssen WPM, Pikkemaat JA, Stapert HR. Preparation of monodisperse polymer particles and capsules by ink-jet printing. *Colloids Surfaces A* 2006;289:96–104.
- Borden MA, Pu G, Runner GJ, Longo ML. Surface phase behavior and microstructure of lipid/PEG-emulsifier monolayer-coated microbubbles. *Colloids Surfaces B* 2004;35:209–223.
- Bouakaz A, de Jong N, Cachard C. Standard properties of ultrasound contrast agents. *Ultrasound Med Biol* 1998;24:469–472.
- Chang MW, Stride EPJ, Edirisinghe MJ. Controlling the thickness of hollow polymeric microspheres prepared by electrohydrodynamic atomization. *J R Soc Interface* 2010;7:S377–S378.
- Chen H, Kreider W, Brayman AA, Bailey MR, Matula T. Blood vessel deformations on microsecond time scales by ultrasonic cavitation. *Phys Rev Lett* 2011;106:034301.
- Chetty K, Stride E, Sennoga CA, Hajnal JV, Eckersley RJ. High-speed optical observations and simulation results of SonoVue microbubbles at low-pressure insonation. *IEEE Trans Ultrasonics Ferroelectr Freq Cont* 2008;55:1333–1342.
- Church CC. The effects of an elastic solid-surface layer on the radial pulsations of gas-bubbles. *J Acoust Soc Am* 1995;97:1510–1521.
- Commander KW, Prosperetti A. Linear pressure waves in bubbly liquids: Comparison between theory and experiments. *J Acoust Soc Am* 1989;85:732–746.
- Glazman RE. Effects of adsorbed films on gas bubble radial oscillations. *J Acoust Soc Am* 1983;74:980–986.
- Gorce J, Arditi M, Schneider M. Influence of bubble size distribution on the echogenicity of ultrasound contrast agents: A study of SonoVue. *Invest Radiol* 2000;35:661–671.
- Hernot S, Klibanov AL. Microbubbles in ultrasound-triggered drug and gene delivery. *Adv Drug Deliv Rev* 2008;60:1153–1166.
- Karshafian R, Bevan PD, Williams R, Samac S, Burns PN. Sonoporation by ultrasound-activated microbubble contrast agents: Effect of acoustic exposure parameters on cell membrane permeability and cell viability. *Ultrasound Med Biol* 2009;35:847–860.
- Kinoshita M, Hynynen K. Key factors that affect sonoporation efficiency in *in vitro* settings: The importance of standing wave in sonoporation. *Biochem Biophys Res Commun* 2007;359:860–865.
- Klibanov AL. Ultrasound molecular imaging with targeted microbubble contrast agents. *J Nucl Cardiol* 2007;14:876–884.
- Kooiman K, Foppen-Harteveld M, der Steen AF, de Jong N. Sonoporation of endothelial cells by vibrating targeted microbubbles. *J Control Release* 2011;154:35–41.
- Leighton TG. *The acoustic bubble*. London: Academic Press; 1994.
- Li TL, Tachibana K, Kuroki M. Gene transfer with echo-enhanced contrast agents: Comparison between Alunex, Optison, and Levovist in mice—Initial results. *Radiology* 2003;229:423–428.
- Li YS, Davidson E, Reid CN, McHale AP. Optimising ultrasound-mediated gene transfer (sonoporation) *in vitro* and prolonged expression of a transgene *in vivo*: Potential applications for gene therapy of cancer. *Cancer Lett* 2009;273:62–69.
- Marmottant P, van der Meer S, Emmer M, Versluis M, de Jong N, Hilgenfeldt S, Lohse D. A model for large amplitude oscillations of coated bubbles accounting for buckling and rupture. *J Acoust Soc Am* 2005;118:3499–3505.
- Marmottant P, Biben T, Hilgenfeldt S. Deformation and rupture of lipid vesicles in the strong shear flow generated by ultrasound-driven microbubbles. *Proc R Soc* 2008;464:1781–1800.
- Martynov S, Stride E, Saffari N. The natural frequencies of microbubble oscillation in elastic vessels. *J Acoust Soc Am* 2009;126:2963–2972.
- Mulvana H, Stride E, Hajnal JV, Eckersley RJ. Temperature dependent behavior of ultrasound contrast agents. *Ultrasound Med Biol* 2010a;36:925–934.
- Mulvana H, Eckersley RJ, Browning R, Tang M, Pankhurst Q, Wells DJ, Stride E. Enhanced gene transfection *in vivo* using magnetic localisation of ultrasound contrast agents. *Proc IEEE Int Ultrason Symp* 2010b (in press).
- Postema M, Van Wamel A, Lancee C, de Jong N. Ultrasound-induced encapsulated microbubble phenomena. *Ultrasound Med Biol* 2004;30:827–840.
- Qin SP, Ferrara KW. Acoustic response of compliant microvessels containing ultrasound contrast agents. *Phys Med Biol* 2006;51:5065–5088.
- Rahim A, Taylor SL, Bush NL, ter Haar GR, Bamber JC, Porter CD. Physical parameters affecting ultrasound/microbubble-mediated gene delivery efficiency *in vitro*. *Ultrasound Med Biol* 2006;32:1269–1279.
- Sarkar K, Shi W, Chatterjee D, Forsberg F. Characterization of ultrasound contrast microbubbles using *in vitro* experiments and viscous and viscoelastic interface models for encapsulation. *J Acoust Soc Am* 2005;118:539–550.
- Sennoga CA, Mahue V, Loughran J, Casey J, Seddon JM, Tang M, Eckersley RJ. On sizing and counting of microbubbles using optical microscopy. *Ultrasound Med Biol* 2010;36:2093–2096.
- Stride E. The influence of surface adsorption on microbubble dynamics. *Phil Trans R Soc A* 2008;366:2103–2115.
- Stride E, Pancholi K, Edirisinghe MJ, Samarasinghe S. Increasing the nonlinear character of microbubble oscillations at low acoustic pressures. *J R Soc Interface* 2008;5:807–811.
- Stride E, Porter C, Prieto AG, Pankhurst Q. Enhancement of microbubble mediated gene delivery by simultaneous exposure to ultrasonic and magnetic fields. *Ultrasound Med Biol* 2009;35:861–868.
- Talu E, Hettiarachchi K, Nguyen H, Lee AP, Powell RL, Longo ML, Dayton P. Lipid-stabilized monodisperse microbubbles produced by flow focusing for use as ultrasound contrast agents. *IEEE Ultrason Symp Proc* 2006;1–5:1568–1571.
- Vlaskou D, Mykhaylyk O, Krotz F, Hellwig N, Renner R, Schillinger U, Gleich B, Heidsieck A, Georg Schmitz G, Hensel K, Plank C. Magnetic and acoustically active lipospheres for magnetically targeted nucleic acid delivery. *Adv Functional Materials* 2010;20:3881–3894.

- Vos H, Dollet B, Bosch JG, Versluis M, de Jong N. Nonspherical vibrations of microbubbles in contact with a wall—A pilot study at low mechanical index. *Ultrasound Med Biol* 2008;34:685–688.
- Vos H, Dollet B, Versluis M, de Jong N. Nonspherical shape oscillations of coated microbubbles in contact with a wall. *Ultrasound Med Biol* 2011;37:935–948.
- Widder K, Flouret G, Senyei A. Magnetic microspheres—Synthesis of a novel parenteral drug carrier. *J Pharm Sci* 1979;68:79–82.
- Zhang M, Fabiilli ML, Haworth KJ, Padilla F, Swanson SD, Kripfgans OD, Carson PL, Fowlkes JB. Acoustic droplet vaporization for enhancement of thermal ablation by high intensity focused ultrasound. *Acad Radiol* 2011;18:1123–1132.